

## Particle physics with petawatt class lasers

By S. KARSCH,\* D. HABS,\* T. SCHÄTZ,\*  
U. SCHRAMM,\* P.G. THIROLF,\* J. MEYER-TER-VEHN,\*\*  
AND A. PUKHOV\*\*

\*Ludwig-Maximilians-Universität München, Sektion Physik, 85748 Garching, Germany

\*\*Max-Planck-Institut für Quantenoptik, 85748 Garching, Germany

(Received 31 July 1998; Accepted 2 December 1998)

With a Petawatt class CPA laser of the LLNL Livermore or the proposed GSI (Darmstadt) type laser, interactions with matter can be studied in the upper  $10^{20}$  W/cm<sup>2</sup> regime. With such a laser focused into an underdense plasma, strong electron bursts with energies up to several 100 MeV are ejected in a forward direction. This leads to a comparable burst of bremsstrahlung radiation in the presence of high-Z material. Here, we discuss the corresponding  $\gamma$ -induced nuclear reactions including secondary particle production, including pions. Due to the threshold behavior in the production, and the advantage of delayed detection, we propose to employ these reactions for probing the initial plasma conditions.

---

### 1. Introduction

The development of high power CPA lasers within the last decade presently culminates in focal intensities above  $10^{20}$  W/cm<sup>2</sup> (Perry & Mourou 1994) and corresponding electric field strengths of  $3 \times 10^{13}$  V/m, implying a fully relativistic electron quiver motion. In this regime, the refractive index of an underdense plasma  $n(r) = 1 - \omega_p^2(\gamma, r)/\omega^2 \cdot [n_e(r)/n_0]$ ,  $r$  being the distance from the beam center, will be influenced in two ways. By ponderomotive expulsion the electron density  $n_e(r)$  will be reduced compared to the background density  $n_0$ , locally increasing  $n(r)$ . Furthermore, the plasma frequency  $\omega_p(\gamma, r) = \sqrt{4\pi e^2 n_0/\gamma(r) m_e}$  is reduced due to the relativistic mass increase  $\gamma(r) m_e$ , also raising the refractive index. If the laser power now exceeds the critical power of  $P_c = 17(\omega/\omega_p)^2$  GW (Sun *et al.* 1987), this focusing effect balances diffraction, keeping the beam focused over many Rayleigh lengths, a process which is referred to as ponderomotive–relativistic self focusing (Monot *et al.* 1995; Pukhov *et al.* 1996; Borghesi *et al.* 1997; Wagner *et al.* 1997; Malka *et al.* 1997).

Moreover, a burst of relativistic electrons is ejected predominantly in laser direction, forming a plasma waveguide (channel) for the co-propagating laser beam (Monot *et al.* 1995; Pukhov *et al.* 1996; Borghesi *et al.* 1997; Wagner *et al.* 1997; Malka *et al.* 1997; Gahn *et al.* 1998). The currents involved reach a strength in the order of the Alfvén current  $I_A = (mc^3/e)\beta\gamma = 17$  kA  $\beta\gamma$ , assuming up to  $5 \times 10^{12}$  electrons in a pulse of about the laser pulse length of 400 fs (Pukhov & Meyer-ter-Vehn 1997). They are surrounded by self-generated circular magnetic fields of the order of 100 MG. Several acceleration mechanisms have been proposed, such as wakefield acceleration (Tajima *et al.* 1979; Wagner *et al.* 1997; Malka 1997) and plasma wave-breaking (Sheng & Meyer-ter-Vehn 1997), or resonant energy transfer to the quivering electrons in an inverse FEL (free electron laser) process (Pukhov & Meyer-ter-Vehn 1998). Nevertheless, the acceleration scheme is not yet fully understood. Moreover, ions are driven out of the channel due to the large space charge generated by the electron density depression.

The large fluxes of high energy electrons and ions give rise to the production of various types of secondary particles (figure 1), which due to their threshold behavior in the production, are optimally suited to probe the conditions inside the channel. We propose to concentrate especially on the delayed reactions and the slow particles that reach particle detectors after a temporal delay, because the tremendous flux of  $\gamma$  rays produced causes severe pile-up in particle detectors. Furthermore, the ultrafast temporal characteristics of the particle radiation and the  $\mu\text{m}$  scale source size could open up new fields of applied research.

## 2. Expected yield of primary electrons

Relativistic 3D PIC simulations using the VLPL code (Pukhov & Meyer-ter-Vehn 1996) calculations of the laser plasma interaction were carried out for focal intensities of  $10^{18} \text{ W/cm}^2$  (1 TW, 150 fs),  $10^{19} \text{ W/cm}^2$  (10 TW, 150 fs),  $10^{20} \text{ W/cm}^2$  and  $10^{21} \text{ W/cm}^2$  (1 PW, 330 fs), corresponding to the presently available intensity at the MPQ (Max Planck Institut für Quantenoptik) ATLAS laser, the ongoing upgrade of this system, and a realistically (spot size  $30 \mu\text{m}$ ), and ideally ( $9 \mu\text{m}$ ) focused petawatt system.

The laser was assumed to be focused into a preformed plasma with an exponential density profile (scale length  $30 \mu\text{m}$ ) reaching from vacuum to  $6n_c$ , with  $n_c$  being the critical density. In figures 2 and 3, the calculated spectra are shown, which can be parametrized by a suprathermal distribution with temperatures of 0.8 MeV, 5 MeV, 12 MeV and 50 MeV, respectively. Compared to experimental data (Gahn *et al.* 1998; Cowan *et al.* 1998), the shape of the spectra matches well in the high energy part. However, for the  $10^{18} \text{ W/cm}^2$  case (Gahn *et al.* 1998), the experimental yield was found to be one order of magnitude lower than the calculated one.

## 3. Secondary particle production processes

We now focus on the nuclear physics processes which can occur in a solid target following the plasma region as partially suggested by Shkolnikov *et al.* (1997). Representing the primary energy loss mechanism for the electron beam, bremsstrahlung is generated with an energy

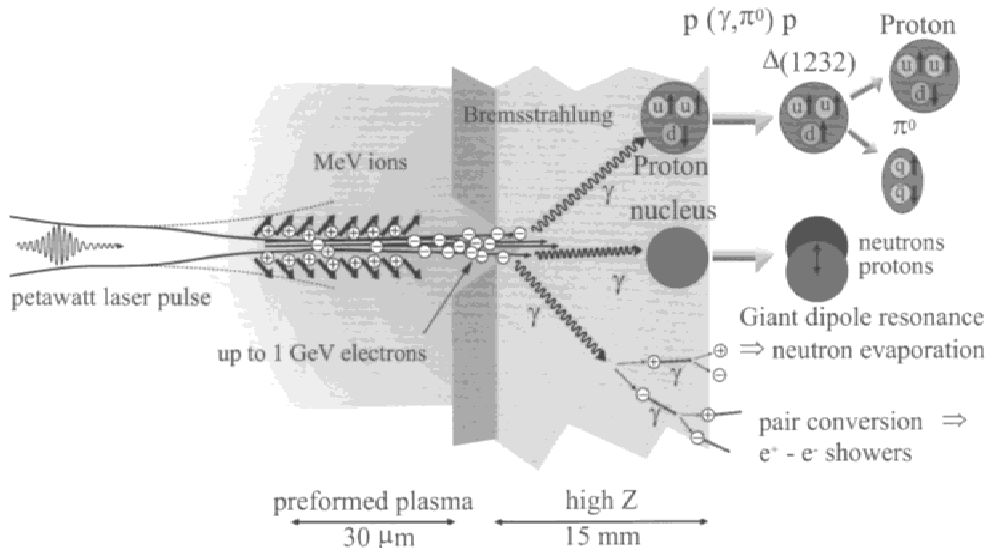


FIGURE 1. Particle production processes triggered by the large electron, ion, and  $\gamma$  fluxes which result from a petawatt laser shot focused into underdense plasma, followed by a solid target. Notice the different scales of plasma and the solid region.

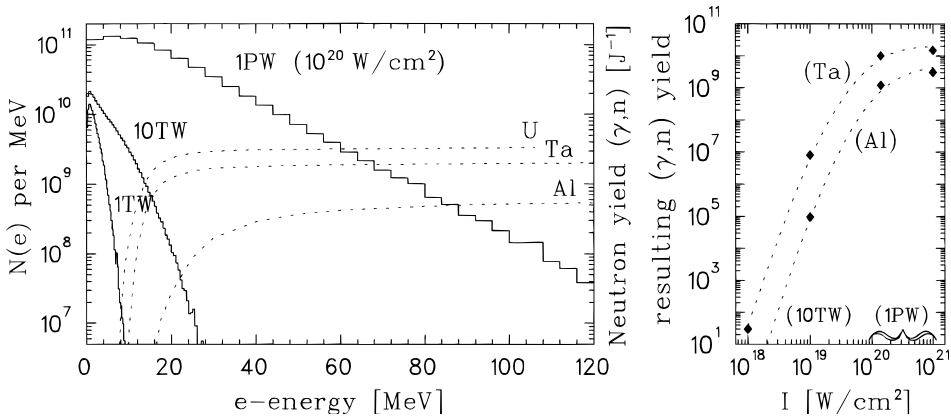


FIGURE 2. Expected electron spectra for laser powers of 1 TW, 10 TW and 1000 TW assuming corresponding intensities of  $10^{18}$  W/cm<sup>2</sup>,  $10^{19}$  W/cm<sup>2</sup> and  $1.4 \cdot 10^{20}$  W/cm<sup>2</sup>. The dashed curves show the neutron yields described in the text for different target materials as a function of the electron energy (Cierjacks 1983). The right curve shows the overall neutron yield/shot in dependence of the laser intensity.

range of nearly the maximum electron energy. In figure 3, the calculated bremsstrahlung spectrum in 8 mm of tungsten for  $10^{21}$  W/cm<sup>2</sup> is shown. The spectrum was calculated numerically using the code GEANT (GEANT Users Guide) and nearly follows the shape of the electron spectrum at an intensity level of 0.1%. Various processes arise from the presence of this large  $\gamma$  flux. In figure 1 the main production reactions are shown. One can easily distinguish the different mechanisms, the one with the lowest threshold being electromagnetic pair production. At somewhat higher energies ( $\gamma, n$ ) reactions will occur, corresponding to the excitation of nuclei in the target. At the highest energies above 320 MeV pion production is expected with a large cross-section, due to the formation of the  $\Delta$ -resonance in the nucleons. Furthermore, Coulomb explosion of the laser channel drives ions of several MeV into radial direction, allowing, for example, fusion reactions in deuterium gas.

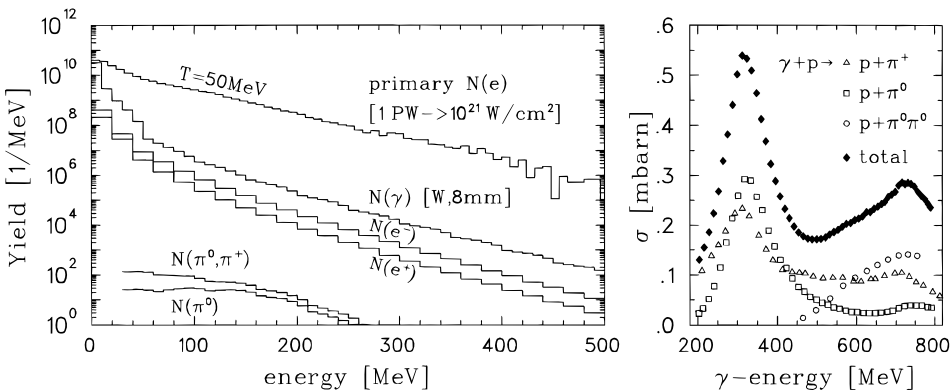


FIGURE 3. Predicted primary electron spectrum ( $T \approx 50$  MeV) for the 1 PW case with stronger focusing ( $10^{21}$  W/cm<sup>2</sup>). The lower curves show the calculated (GEANT simulation) bremsstrahlung  $\gamma$ -yield and the electron and positron distribution after 8 mm of tungsten foil, representing about two radiation lengths. Also, a still relevant production of several thousand pions per shot is sketched in the two lowest curves. (right) The cross section for photopion production via the  $\Delta(1232)$ -spinflip resonance of the nucleon, at an energy of 294 MeV. Due to kinematics, the resonance is shifted to 310 MeV in the laboratory framework (Metag 1998).

### 3.1. Neutron production via $(\gamma, n)$ reactions with nuclei

For  $\gamma$ -energies as low as 1.67 MeV, the cross-section for  ${}^9\text{Be}(\gamma, n){}^8\text{Be}$  shows a narrow resonance of 1.3 mbarn, followed by a broad resonance of 2.7 mbarn centered at energies of 20 MeV with a FWHM of 10 MeV (Nuclear Physics Data Center). For the  $10^{18}$  W/cm<sup>2</sup> case the expected neutron yield of  $5 \times 10^4$ /shot already represents a significant amount of neutrons at comparably low intensities.

For heavy nuclei,  $(\gamma, n)$ - and  $(\gamma, f)$ -giant resonances with a peak cross section of the order of 0.1–1 barn are centered around 15 MeV with a FWHM of 5 MeV. These resonances correspond to a collective dipole oscillation of the protons against the neutrons in the nucleus, as outlined in figure 1. Since the excitation energy lies well beyond the evaporation energy for a single nucleon of 8 MeV, the resonance primarily decays by emission of one or two nucleons.  $(\gamma, n)$  and  $(\gamma, f)$  reactions in heavy targets can be employed for diagnostics especially at intensities of  $10^{19}$  W/cm<sup>2</sup> to  $10^{20}$  W/cm<sup>2</sup> due to their threshold behavior depicted in figure 2. In the  $10^{21}$  W/cm<sup>2</sup> case, one expects about  $10^{10}$  n/shot with very sharp temporal characteristics, offering a unique tool for time resolved neutron physics. These neutrons are emitted at energies of a few MeV ( $\beta \approx 0.1 c$ ) and therefore by means of a time-of-flight technique are easily distinguishable from the much faster bremsstrahlung  $\gamma$  rays.

### 3.2. Pion production via the $\Delta$ -resonance

At  $10^{21}$  W/cm<sup>2</sup>, the electron and also the  $\gamma$ -spectrum is predicted to have a temperature of 50 MeV, so that further processes will be allowed. The lowest excited state of the nucleon, the  $\Delta(1232)$  spin flip resonance of the valence quarks in the nucleon, is located around a  $\gamma$ -energy of 310 MeV. The resonance is observed independent of charge in protons ( $\Delta^+$ ) as well as in neutrons ( $\Delta^0$ ) at nearly the same energy. The maximum cross section amounts to 0.3 mbarn. It can be excited by  $\gamma$  rays of appropriate energy and decays primarily into a nucleon and a pion, which can be detected. In the right part of figure 3, the cross section for  $(\gamma, \pi)$ -production (Metag 1998) via  $\Delta^{+,0}$  is shown for different pion channels. The calculated pion yield, together with primary and secondary electron and  $\gamma$ -radiation, is shown in the left part of figure 3 for the  $10^{21}$  W/cm<sup>2</sup>, 1 PW case, indicating an overall number of several thousand pions per shot. However, since the half-life of the charged pions for the decay into a muon and its neutrino is only  $2.6 \times 10^{-8}$  s, ( $\approx 5 \times 10^{-8}$  s in the laboratory framework), it is difficult to measure the pions directly in the vicinity of the  $\gamma$ -flash. The neutral pion decays into 2 photons after  $8 \times 10^{-17}$  s, so it will not contribute to a measurable signal, and most negative pions are captured by target nuclei. A promising approach is to look for the decay of the stopped muons into positrons after  $2.2 \times 10^{-6}$  s. A possible target geometry may consist of a low  $Z$ -electron production target combined with a high  $Z$  bremsstrahlung radiator, enclosed in a high  $Z$ -cylinder for production and stopping of pions. The muon should then be stopped inside a scintillator, placed around the cylinder in a nearly  $4\pi$  geometry. The signature of a  $\pi^+$  will be a delayed high energy positron and, if stopped in the scintillator, two 512 keV photons. This experimental approach could therefore be used to probe the highest energy part of the electron spectrum without being affected by the high  $\gamma$  background.

### 3.3. Production of leptonic showers

At  $\gamma$ -energies beyond 1 MeV, pair production in the vicinity of nuclei takes place. The production cross section scales like  $\sigma_p \propto Z^2 \ln E_\gamma$  for  $E_\gamma$  between 2.5 and 25 MeV and with a slower increase with  $E_\gamma$  at higher energies. If the pairs produced have sufficient energy, they will again produce bremsstrahlung above 1 MeV, so that depending on the primary energy, a shower is created (Amaldi 1981). The shower spectrum as plotted in figure 3 was calculated numerically using the GEANT code, amounting to about 10% of the  $\gamma$  yield.

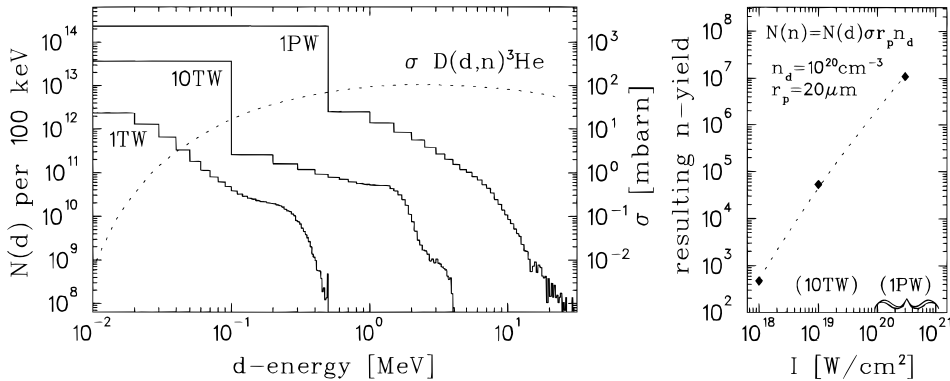


FIGURE 4. Calculated (with VLPL code) deuteron ion spectra for the 1 TW, 10 TW and 1000 TW cases discussed above. The dashed line represents the deuteron fusion cross section. The right curve shows the expected fusion neutron yield/shot for different focal intensities. The preplasma region was assumed to have a homogeneous density of  $10^{20}$  d/cm<sup>3</sup> over a length of 20  $\mu$ m according to Pretzler (1998).

### 3.4. Production of neutrons via $d(d,n)^3He$ fusion reactions

As shown in figure 1, by the space charge of the low electron density in the channel, ions of several MeV are driven into radial direction. In order to investigate the initial ion distribution, it is convenient to determine the neutron energy spectrum from the  $d(d,n)^3He$  fusion reaction. Its cross section is shown in figure 4, together with calculated ion distributions. For the total yield depicted in the right part of figure 4 the same preplasma conditions as in Pretzler *et al.* (1998) was used. The fusion neutrons are monoenergetic (2.45 MeV) in the center-of-mass system, but due to kinematics, one observes a shifted and broadened spectrum, from which the initial ion spectrum can be deduced. First measurements (Norreys *et al.* 1998; Pretzler *et al.* 1998) were performed at the ATLAS laser, focused into a preformed  $d$ -plasma with an exponential density profile of 30  $\mu$ m, yielding 130 neutrons/shot. With a petawatt class laser, one would expect  $10^7$  neutrons/shot from the predicted ion spectra. Employing this mechanism and  $(\gamma,n)$  reactions, a source of neutrons with extreme brilliance (small source volume) and ultrafast temporal characteristics can be envisioned for a new class of experiments.

## REFERENCES

- AMALDI, U. 1981 *Physica Scripta* **23**, 409.  
 BORGHESI, M. *et al.* 1997 *Phys. Rev. Lett.* **78**, 879.  
 COWAN, T.E. *et al.* 1998 *Proc. of Int. Conf. on Lasers 1997* (Soc. Opt. and Quant. Electron, McClean, VA) and private communication.  
 EDGE, R.O. *et al.* 1957 *Nucl. Phys.* **2**, 485.  
 FUJIEHIRO *et al.* 1982 *Can. J. Phys.* **60**, 1672.  
 GAHN, C. *et al.* 1998 *Appl. Phys. Lett.* (in press).  
 GEANT Users guide, R. Brun *et al.* ed. CERN Report No. DD/EE/82 (unpublished).  
 KNIEVEL, V. *et al.* 1975 *Nucl. Phys. A*, **247**, 91.  
 MALKA, G. *et al.* 1997 *Phys. Rev. Lett.* **79**, 2053.  
 MOMOT, P. *et al.* 1995 *Phys. Rev. Lett.* **74**, 2953.  
*Neutron Sources for Basic Physics and Application*, 1983, 81ff S. Cierjacks, ed. (Pergamon Press, Oxford).  
 NORREYS, P.A. *et al.* 1998 *Plasma Phys. Controlled Fusion* **40**, 175.  
 Nuclear Physics Data Center, Brookhaven Nat. Lab.  
 PERRY, M.D. & MOUROU, G. 1994 *Science* **264**, 917.

- PRETZLER, G. *et al.* 1998 *Phys. Rev. E* **58**, 1165.
- PUKHOV, A. *et al.* 1996 *Phys. Rev. Lett.* **76**, 3975.
- PUKHOV, A. & MEYER-TER-VEHN, J. 1996 *APS Bull.* **41**, 1502.
- PUKHOV, A. & MEYER-TER-VEHN, J. 1997 *Phys. Rev. Lett.* **79**, 2686.
- PUKHOV, A. & MEYER-TER-VEHN, J. 1998 *Phys. Plasmas* **5**, 1880.
- SHENG, ZH.M. & MEYER-TER-VEHN, J. 1997 *Phys. Plasmas* **4**, 493.
- SHKOLNIKOV, P.L. *et al.* 1997a *J. Nonl. Optic. Phys. Mat.* 161.
- SHKOLNIKOV, P.L. *et al.* 1997b *Appl. Phys. Lett.* **71**, 3471.
- SUN, G.Z. *et al.* 1987 *Phys. Fluids* **30**, 526.
- TAJIMA, T. *et al.* 1979 *Phys. Rev. Lett.* **43**, 267.
- WAGNER, R. *et al.* 1997 *Phys. Rev. Lett.* **78**, 3125.